PNAS
www.pnas.org

Supplementary Information for

Label-free adaptive optics imaging of human retinal macrophage distribution and dynamics

Daniel X. Hammer[1,*], Anant Agrawal[1], Ricardo Villanueva[2], Osamah Saeedi[2], and Zhuolin Liu[1,*]

[1]Division of Biomedical Physics, Office of Science and Engineering Laboratories, Center for Radiological Devices, Food and Drug Administration, 10903 New Hampshire Avenue, Silver Spring MD 20993
[2]Department of Ophthalmology and Visual Sciences, University of Maryland School of Medicine, 419 W. Redwood Street, Baltimore MD 21201

Corresponding authors: *daniel.hammer@fda.hhs.gov and zhuolin.liu@fda.hhs.gov

This PDF file includes:

Supplementary text
Figures S1 to S6
Tables S1 to S2
SI References
Captions for Movies S1 to S5

Other supplementary materials for this manuscript include the following:

Movies S1 to S5

Supplementary Information

SI Materials and Methods

Criteria used to identify ILM macrophage cells

ILM macrophage cells were counted manually in the AO-OCT volumes by two graders independently using custom counting software and the following criteria. AO-OCT volumes were scanned in three dimensions and macrophage cells counted only when found within 10 μm of the ILM. In a few cases macrophage cells were found further into the vitreous (within 25 μm of the ILM), but these cells were excluded from the final count. The hyper-reflective soma and processes of ILM macrophage cells could be identified in the majority of subjects (16 of 19) upon visual examination. When soma and processes were both resolved, the location of the soma was marked to record distribution. In some subjects, especially younger subjects with hyperreflective ILM, processes were difficult to distinguish from the background and only cell body locations were used. Care was taken to avoid spurious hyper-reflective regions that could be misclassified as macrophage soma, particularly above vessels, but also including Gunn's dots, activated retinal astrocytes and Müller cells (ARAM), epiretinal membrane, and other cellular debris [1]. Although processes between adjacent ILM macrophage cells did make contact, there was no significant overlap in the regions they probed (unlike astrocytes, which are known to occupy significantly overlapping regions with respect to their nearest neighbor [2]). If these hyperreflective structures were in the correct location (within 5-10 μm of the ILM), had non-uniform reflectance across their soma, and had a size slightly enlarged from the average ramified macrophage soma size, these were generally classified as ILM macrophage cells. However, such cases made up a significant minority (<5%) of all cells counted.

After the two graders independently counted the ILM macrophage cells, custom software compared the location and counts for agreement (allowing some tolerance for small deviations in soma location chosen by the graders). Both graders then independently recounted the structures where there was disagreement, knowing the locations chosen by the other reader. Because there was still some disagreement between the two graders after the secondary examination of structures, the final counts presented in this paper were the counts averaged for the two graders, while the distribution maps were from one grader. This grading process, with two rounds of manual review where the second-round counts were informed by the other grader, was designed to produce the most accurate counts, mitigating undercounting that would occur if the counts for the structures where there was disagreement were discarded after the first review round. It also provided a manual check of the location agreement tolerance.

Conditions required to resolve and track ILM macrophage processes

There exists a trade-off between the number of AO-OCT volumes averaged to resolve individual processes and the temporal sampling required to track individual processes for further quantification. Acquisition temporal sampling (i.e., time to decorrelate) and image averaging were optimized to resolve and track ILM macrophage processes. We explored the decorrelation associated with ILM macrophage process motion by imaging a 33-year-old healthy subject at a single location (12T) continually over the course of ~20-25 minutes with fine temporal sampling. We acquired 65 volume sets (15 volumes/set collected over 6.5 s) with a temporal spacing of ~18 s (0.3 min). The time between each acquisition (~12 s) is required to write the data to disk, allow the subject to blink and rest, reset subject alignment, and reset DM focus (if needed). This time (18 s) represents the approximate minimum temporal spacing for sets of 10-15 volumes and our volume rate. Greater than 800 total usable volumes without blinks or excessive motion were registered in three dimensions and each of the 65 sets of 15 volumes was averaged individually. An *en face* OCT image of ILM macrophage cells was extracted from each set and combined to create a time-lapsed video. Sub-pixel accuracy 3-D registration was completed using a reference frame, and the cross-correlation was calculated between the reference frame and the other frames in the time-lapsed video for regions-of-interest (ROI) centered on 12 ILM macrophage cells (100×100 pixels) and three background regions (50×50 pixels) where no ILM macrophage cells existed. The cross-correlation coefficient was calculated in a manner similar to that used for

RPE motility [3]. The cross-correlation established a temporal spacing (Δt) cutoff, whereby any spacing between adjacent frames greater than the cutoff was not used in the average v_p calculation.

We further examined the effect of averaging on ILM macrophage process resolution by similarly imaging a 49-year-old healthy subject with relatively good fixation at a single location (10.5T) repeatedly over the course of ~20-25 minutes. We acquired 31 volume sets (10 volumes/set collected over 4.3 s at 2.33 volumes/s) with a temporal spacing of ~0.3–2 min. A total of 276 volumes were collected and registered in three dimensions, and *en face* averages of the ILM macrophage cells and GCL were created over increasing time durations for further analysis.

Reproducibility of fast ILM macrophage dynamics

The reproducibility of the fast-dynamic measurement was examined by measuring process velocity at the same retinal location in three subjects across durations from 1.5 to 7 months. Although the processes that were counted were chosen for their visibility, in many cases the same processes from the same ILM macrophage cells were tracked across the respective imaging durations.

AO imaging of glaucoma subjects with hemifield defects

In 6 glaucoma subjects and 6 age-matched control subjects, we compared ILM macrophage density at six locations in the temporal field, symmetric about the horizontal meridian (3T2.5S, 3T2.5I, 6T2.5S, 6T2.5I, 12T2.5S, 12T2.5I, Fig. S1A) to compare results to the hemifield defect in the glaucoma subjects (Fig. 5G). At each location, 300 AO-OCT volumes were collected over 15-20 minutes, allowing the opportunity to examine ILM macrophage process motility in the locations where there were significant numbers (Table 2).

Statistical Methods

Analysis of variance (ANOVA) was used to determine if there was significant difference in ILM macrophage density among the mean age groups separated by decade (Fig. 2E). Linear regression analysis was used to determine the rate of ILM macrophage cell loss and correlation between the total number of cells and age in the control cohort (Fig. 2D) and all subjects (Fig. 5F). Student's t-test was used to calculate differences in average ILM macrophage density (Fig. 5F inset) and symmetry (Figs. 5D and S4D) between control and glaucoma cohorts for the distribution experiment; and between inferior and superior regions (control cohort), more normal and hemifield defect regions (glaucoma cohort), and early and moderate glaucoma subjects for the glaucoma experiment (Fig. 5G). Excel was used for all statistical analysis.

SI Results

Subject demographics

The subject demographics are shown in Table S1.

Table S1: Subject demographics

		Glaucoma	Control
Number		6	16
Age		58.1±4.5	45.2±15.4
Race	White	3 (50%)	11 (69%)
	Non-white	3 (50%)	5 (31%)
Sex	Male	1 (16.7%)	11 (69%)
	Female	5 (83.3%)	5 (31%)

Comparison of imaging modes

Since ILM macrophage cells have been previously resolved with both AO-OCT [4, 5] and AOSLO [6], we found it useful to compare imaging modes in the same subject at the same eccentricity using our multimodal imager that has capabilities for both modes [7]. Figure S2 shows a comparison of AOSLO and AO-OCT images acquired from our multimodal AO system. Movie S4 shows the time-lapsed AO-OCT video from this subject. In Fig. S2B, the

number of AO-OCT volumes averaged (169) was similar to the number of AOSLO frames averaged (180) in Fig. S2A. Because the AOSLO frame rate (27 frames/s) is much higher than the AO-OCT volume rate (2.3 vol/s), Fig. S2C also shows the case where the AO-OCT image acquisition duration was similar to that for the AOSLO acquisition. In both cases, while somas are visible in both modes (labeled), processes were visible only in the AO-OCT volume, presumably owing to that mode's axial sectioning capability. Macrophage soma could only be resolved in a few young control subjects using AOSLO.

ILM macrophage distribution and directionality in healthy subjects

ILM macrophage distribution for all healthy control subjects is shown in Fig. S3. Example AO-OCT images near the temporal peak in four subjects of various ages are shown in Fig. S3A. Distribution maps for all healthy control subjects across five decades are shown in Fig. S3B. ILM macrophage density was observed to decrease with aging in the healthy control subjects.

ILM macrophage cells were summed in each quadrant and symmetry was calculated as the maximum proportion among the four quadrants. Symmetry maps display the directionality magnitude where perfect symmetry is represented by a diamond shape (i.e., symmetry of 0.25 in all four directions) and elongation in one of four axes represents preferential presence or accumulation of ILM macrophage cells in that direction. ILM macrophage symmetry is shown in Fig. S4. While some healthy control subjects had higher ILM densities in one specific quadrant (Fig. S4B-C), ILM macrophage distribution was relatively symmetrical for healthy control subjects regardless of age (Fig. S4C-E). Only 3/15 (20%) of subjects had symmetry >0.5 in any one direction. The mean (± standard deviation) symmetry for the healthy control subjects is 0.46 ± 0.11.

ILM macrophage dynamics and image averaging

Movies S2, S3 and S4 show average time-lapsed videos for three control subjects. The average time-lapsed videos are reduced from the original set with greater temporal averaging to smooth the appearance and reduce noise and registration artifacts (e.g., black horizontal stripes) in the video frame (compare Movies S1 and S2 from the same subject and session).

The effect of averaging on ILM macrophage process resolution is shown in Fig. S5, where *en face* average intensity projection AO-OCT images from the GCL (10 µm) and just above the ILM (10 µm) are shown for one healthy subject (4136) with good fixation. RGC somas are fully resolved by ~30 volumes and show monotonic improvement in SNR with volumes averaged (*n*). Conversely, ILM macrophage processes are resolved with less averaging – by ~5-10 volumes (~0.05 min) – but blur with motility after ~50 volumes (~1 min, Fig. S5B) as the acquisition duration for all averaged scans exceeds the time the processes are relatively stationary (seconds to tens of seconds). Note also the increase in apparent ILM macrophage soma size with averaging.

The motion blur can be demonstrated quantitatively by looking at the cross-sectional profile across ILM macrophage processes. We selected one process for each ILM macrophage cell and calculated the mean profile from five adjacent cross-sections. The ROIs are shown in Fig. S5C and the mean cross-sectional profiles for one ILM macrophage process are shown in Fig. S5D across all average *en face* projections. Figure S5E shows the full-width half maximum (FWHM) process diameter for the five ILM macrophage processes as a function of volumes averaged. At 81 volumes averaged (~6 min), the process diameter begins to increase from blurring and for excessive averaging both the mean and standard deviation increase substantially. Thus, optimal resolution of processes occurs when averaging ~5 to 30 volumes up to a duration of ~1 min.

Taken together, the results presented in Figs. 3C and S5 suggest a maximum temporal resolution limit of ~0.5 min to optimally resolve and quantify ILM macrophage processes. In terms of the spatial resolution to do the same, our results suggest that an isotropic resolution on the order of a few microns is required, which can be achieved most optimally with AO-OCT [8]. Macrophage images were created by segmenting the region 10 µm above the ILM, which was made possible by OCT axial sectioning capabilities, and AO-enabled micron-level lateral spatial resolution. The evidence suggests that ILM macrophage cells are predominantly confined to this region and

it is probably that processes will not be resolved outside of the depth-of-focus of the imaging system. Careful placement of system focus in the NFL-GCL near the ILM thus ensures optimal resolution of ILM macrophage cells.

Movie S5 show a time-lapsed video of ILM macrophage cells for a glaucoma subject over a relatively short time duration. No qualitative difference in ILM macrophage dynamics was observed, though slight differences were found in process velocity and coverage area (Table 2).

Reproducibility of ILM macrophage dynamic measurements

Three subjects were imaged over two sessions with 1.5-7 months between sessions to test the reproducibility of the ILM macrophage process velocity measurement. The results are shown in Table S2, where a total of 84 processes (from 40 macrophage cells) were tracked. The average difference in velocity measurement was 1.1 µm/min (range: 0.6 – 2.1 µm/min), or 7% of the average velocity, and the average difference in area was 82 μm^2 (18% of average), indicating good reproducibility.

Table S2: ILM macrophage process velocity and coverage area reproducibility.

Subject	**Date**	**Cells**	**Processes**	**Density** [mm^{-2}]	v_p**(avg±SD)** [µm/min]	v_p**(max)** [µm/min]	**A(avg±SD)** [μm^2]	**A(min)** [μm^2]	**A(max)** [μm^2]	**t(avg±SD)** [min]
8009	3/6/20	10	20	78.7	16.0±11.0	72.0	738±357	138	1478	0.30±0.07
	1/22/20	12	26	68.2	18.1±14.0	83.4	546±356	155	1682	0.26±0.06
6581	3/11/20	5	12	63.0	13.5±9.3	57.3	228±167	82	668	0.32±0.08
	11/20/19	6	10	63.0	14.2±10.9	73.2	251±177	66	683	0.27±0.08
4136	2/26/20	3	6	31.5	15.5±12.4	77.3	471±125	303	668	0.32±0.07
	7/17/19	4	10	26.2	16.1±11.3	59.9	442±240	133	755	0.31±0.09
Total		**Σ=40**	**Σ=84**		**Δ=1.1±0.84**		**Δ=82±96**			

Evidence of reactive ILM macrophage cells

In some older control and glaucoma subjects, there was some evidence of the presence of reactive ILM macrophage cells at the ILM. Figure S6 shows examples of putative reactive ILM macrophage cells taken from three older control subjects and one glaucoma subject. In the *en face* view, there is clear evidence of processes in the ramified ILM macrophage cells, while the nearby reactive ILM macrophage cells have a slightly large, heterogeneously-reflective soma and no evidence of processes, indicating possible retraction of processes. The cross-sectional views indicated that ramified macrophage soma tend to reside further from the ILM (Fig. S6A, C, E, G), while reactive macrophage cells make closer contact with the ILM (Fig. S6B, D, F, H). It is also possible that these structures are another type of macrophage (e.g., true vitreous hyalocytes), though it would be surprising if we observed no reactive macrophage cells in all the locations we imaged. Confirmation of the reactive state of ILM macrophage cells requires further time-lapsed analysis.

SI References

1. D. X. Hammer, Z. Liu, J. Cava, J. Carroll, O. Saeedi. On the axial location of Gunn's dots. *Am J Ophthalmol Case Reports*, **19**,100757 (2020).
2. C. Distler, H. Weigel, K. P. Hoffmann. Glia cells of the monkey retina: I. Astrocytes. *J Comp Neurology* **333**(1), 134-147 (1993).
3. Z. Liu, K. Kurokawa, D. X. Hammer, D. T. Miller. In vivo measurements of human RPE cells motility. *Biomed Opt Express* **10**(8), 4142-4158 (2019).
4. Z. Liu, K. Kurokawa, F. Zhang, J. J. Lee, D. T. Miller. Imaging and quantifying ganglion cells and other transparent neurons in the living human retina. *Proc Natl Acad Sci U.S.A.* **114**(48), 12803–12808 (2017).
5. K. Kurokawa, J. A. Crowell, F. Zhang, D. T. Miller. Suite of methods for assessing inner retinal temporal dynamics across spatial and temporal scales in the living human eye. *Neurophoton* **7**(1), 015013 (2020).

6. S. A. Burns, A. E. Elsner, K. A. Sapoznik, R. L. Warner, T. J. Gast. Adaptive optics imaging of the human retina. *Prog Retin Eye Res* **68**, 1-30 (2019).
7. Z. Liu, J. Tam, O. Saeedi, D. X. Hammer. Trans-retinal cellular imaging with multimodal adaptive optics. *Biomed Opt Express* **9**(9), 4246-4262 (2018).
8. M. V. Castanos, D. B. Zhou, R. E. Linderman, R. Allison, T. Milman, J. Carroll, J. Migacz, R. B. Rosen, T. Y. P. Chui. Imaging of macrophage-like cells in living human retina using clinical OCT. *Invest Ophthalmol Vis Sci* **61**(6), 48 (2020).

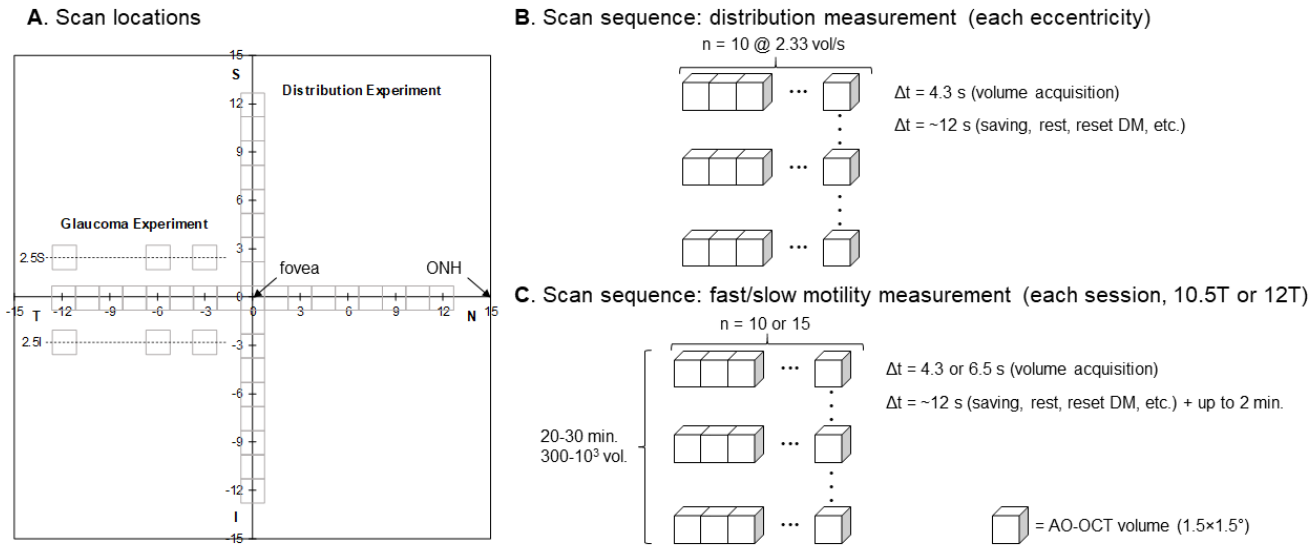

Fig. S1. Scan distribution and sequences collected for measurement of ILM macrophage distribution and motility. (A) Non-overlapping AO-OCT volumes were collected across the horizontal and vertical meridians at a spacing of 1.5° for the distribution experiment. Six additional locations 3°, 6°, and 12° on the temporal size and 2.5° above and below the meridian were collected to examine ILM macrophage characteristics in glaucoma subjects with hemifield defect. (B) For the distribution measurement three sets of 10 volumes were collected at each location. (C) For the fast and slow motility measurements, sets of 10 or 15 volumes were collected continually for 20-30 minutes at 10.5T or 12T. For slow motility, this was repeated over days to months to measure ILM macrophage migration.

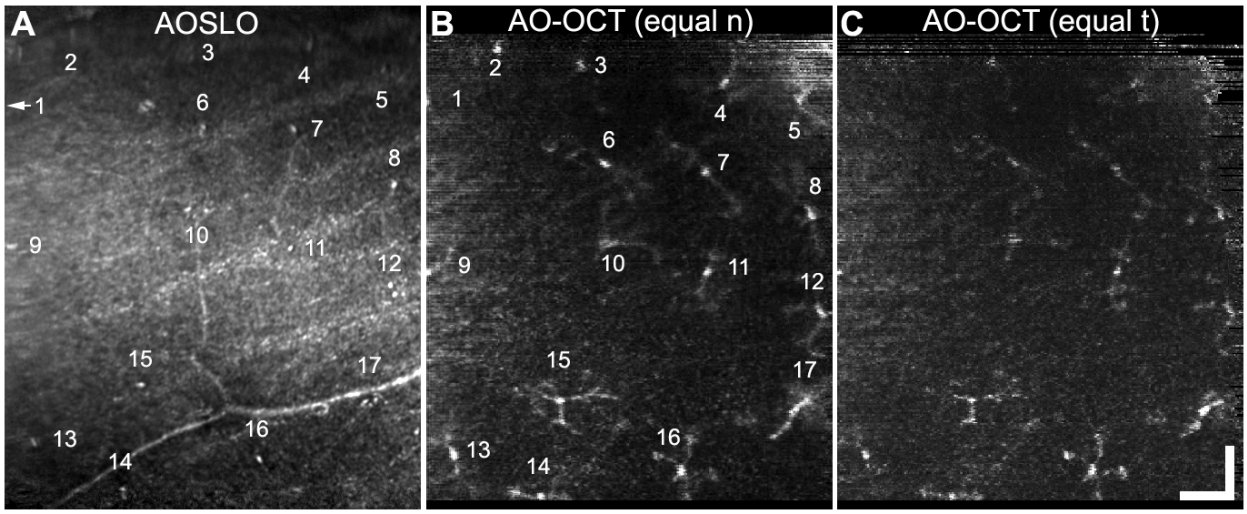

Fig. S2. ILM macrophage soma can be resolved with AOSLO and AO-OCT. ILM macrophage somas (hyper-reflective regions) resolved with AOSLO (A), and somas and processes resolved with AO-OCT (B, C) in one 24-year-old healthy control subject. In (B), the number of AO-OCT volumes averaged was similar to the number of AOSLO frames averaged in (A). In (C), the total duration (~7 sec.) of the AO-OCT and AOSLO acquisitions were similar. Labels refer to corresponding 17 ILM macrophage cells confirmed in the time-lapsed AO-OCT volume (Movie S4). Scalebars = 50 µm.

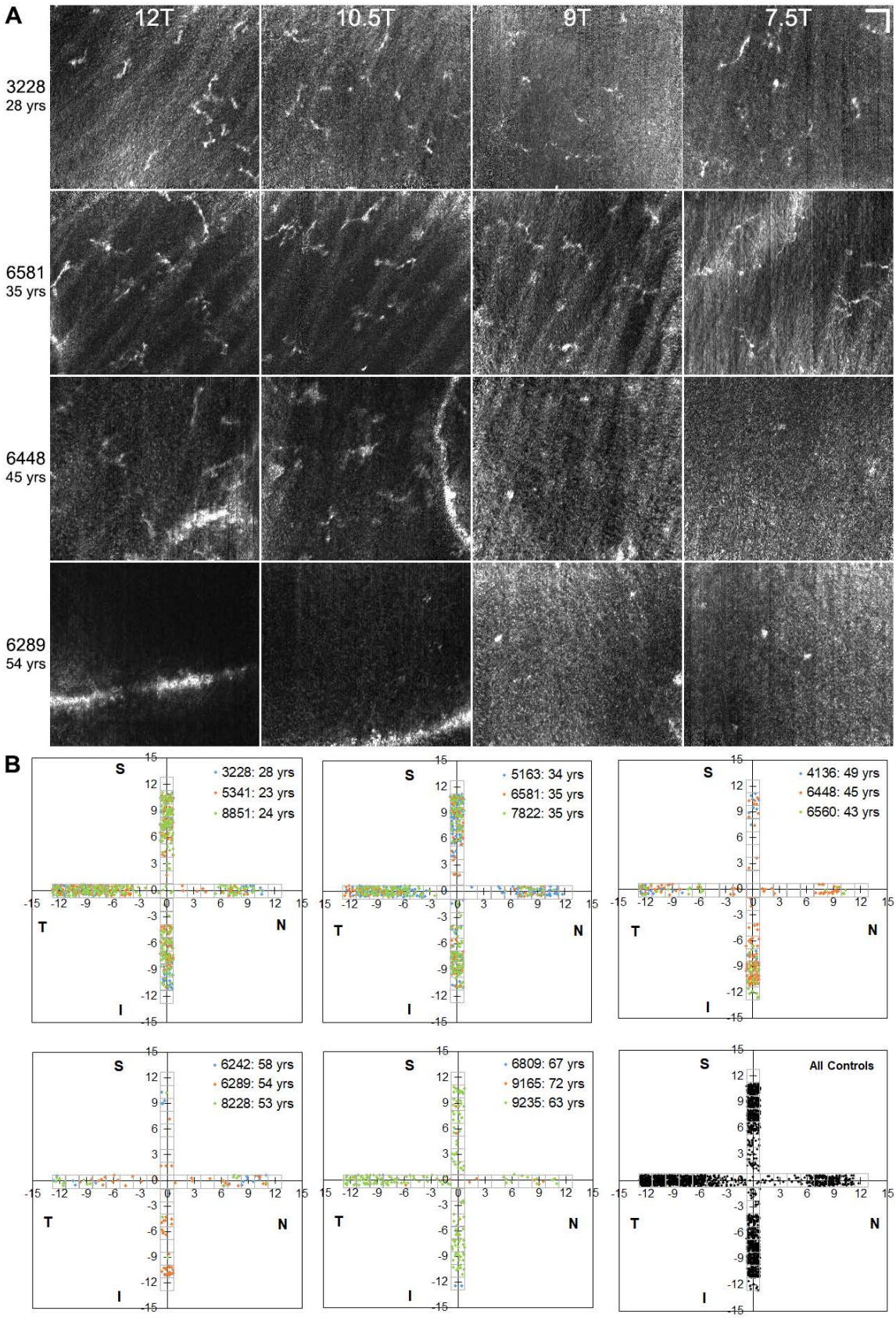

Fig. S3. ILM macrophage distribution decreases with age. (A) Example *en face* AO-OCT axial projections near the temporal peak in a four healthy control subjects over four decades. Scalebars = 50 µm. (B) Distribution maps for all healthy control subjects and separated by decade.

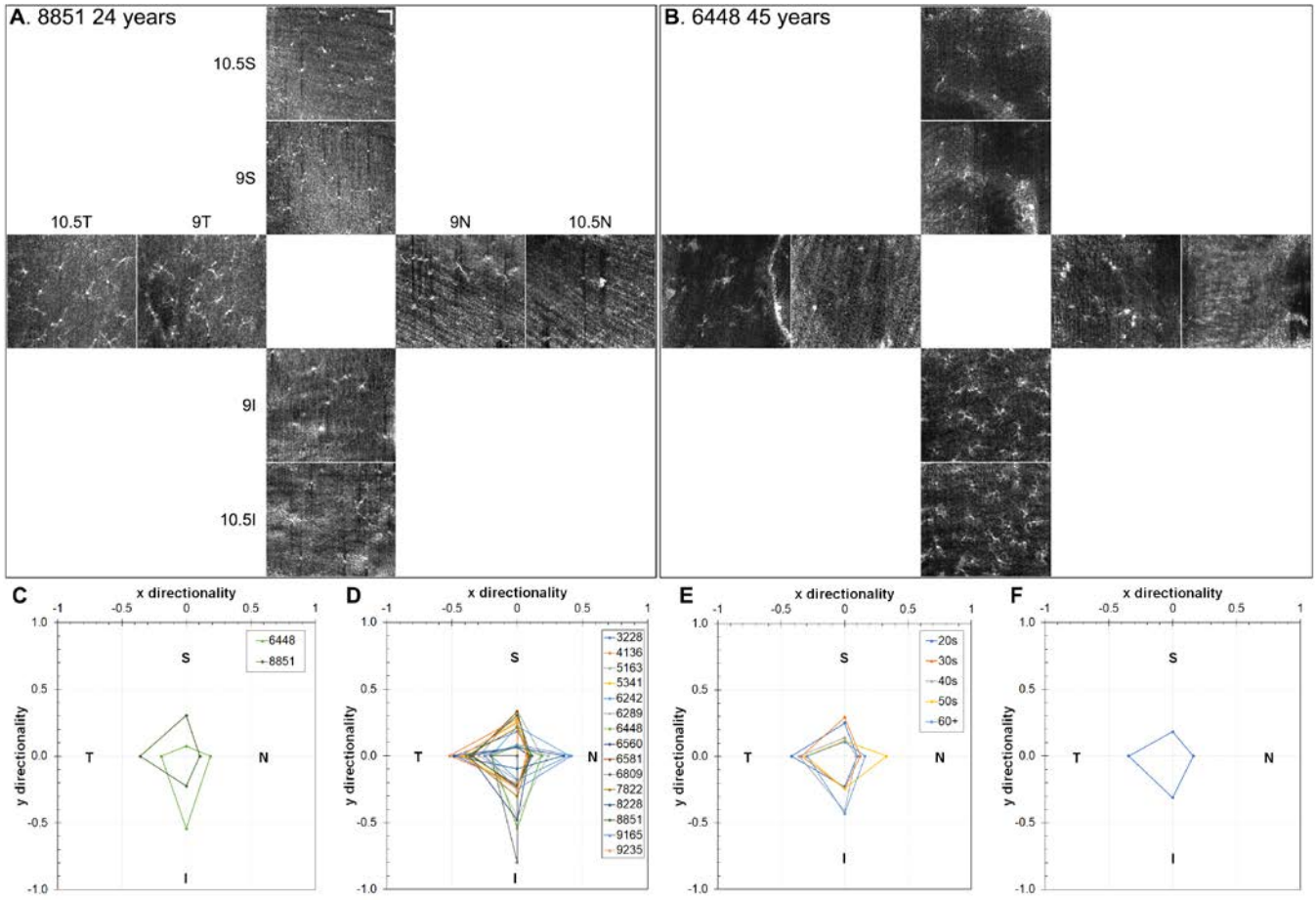

Fig. S4. **ILM macrophage distribution is relatively symmetrical in healthy control subjects.** Example *en face* AO-OCT axial projections near the peak in four quadrants in (A) one 24-year-old and (B) one 45-year-old healthy control subject. Scalebar = 50 µm. The middle-aged subject (6448) had atypical asymmetric ILM macrophage distribution with accumulation in the inferior direction (C). Symmetry plots for: (D) individual healthy control subjects, (E) segmented by decade of age, and (F) mean of all healthy control subjects.

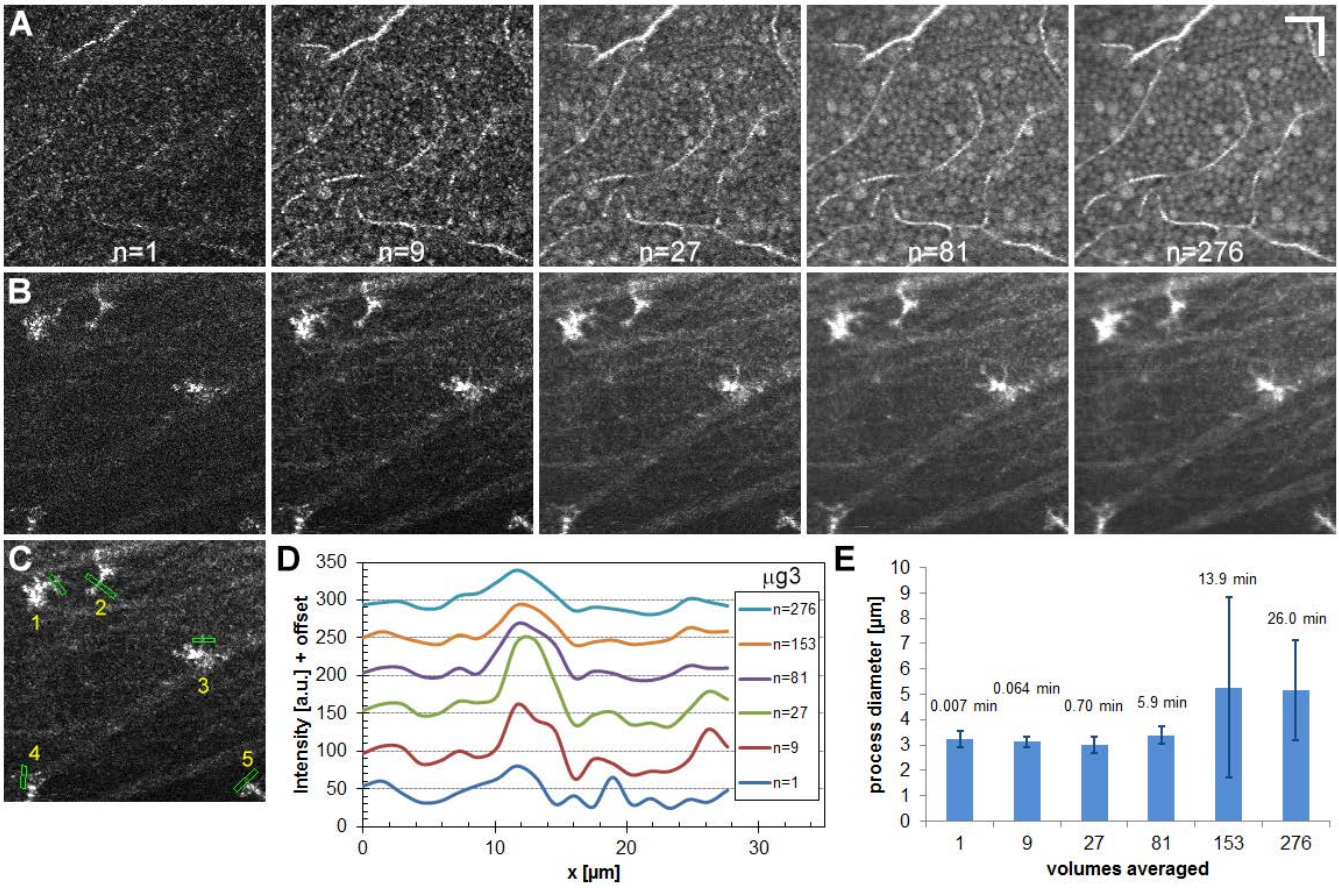

Fig. S5. **ILM macrophage process resolution is sensitive to averaging.** Average AO-OCT *en face* projections of: (A) GCL and (B) ILM macrophage cells for 1, 9, 27, 81, and 276 frame-averages for one healthy subject with good fixation. (C) ROIs for mean cross-sectional profiles across five processes of five ILM macrophage cells. (D) Mean cross-sectional profiles as a function of averaging for ILM macrophage 3 in (C). (E) Mean FWHM process diameter for five processes shown in (C), where error bars indicate ±SD. Scalebar = 50 µm.

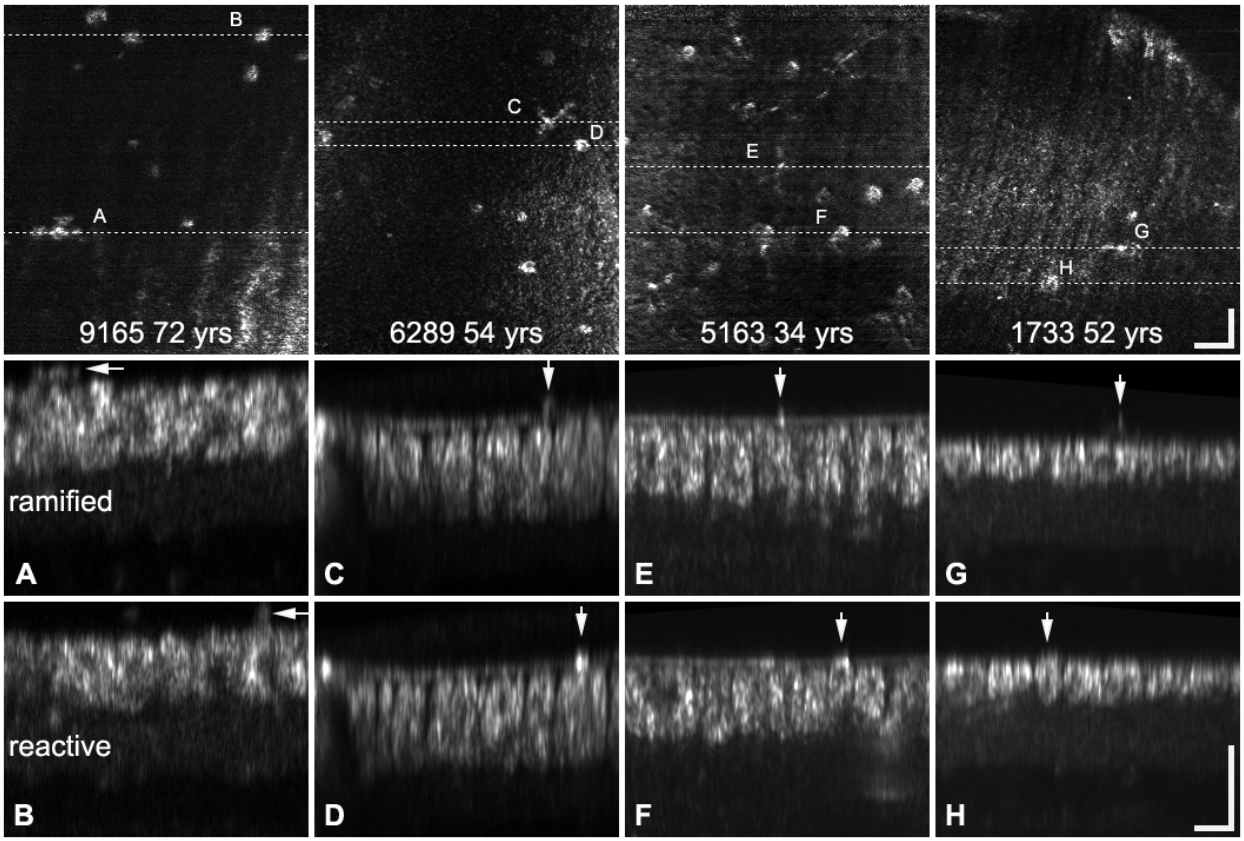

Fig. S6. Evidence of reactive ILM macrophage cells in older subjects. Comparison of ramified and potential reactive ILM macrophage cells in three healthy control subjects and one glaucoma subjects. Top row: *en face* AO-OCT projections (10 µm above ILM) show a variety of macrophage shapes. Dotted lines are locations of cross-sectional frames shown in bottom rows. Middle row (A, C, E, G): cross-sectional AO-OCT projection of ramified ILM macrophage cells. Bottom row (B, D, F, H): cross-sectional AO-OCT projection of potential reactive ILM macrophage cells. Scalebar = 50 µm.

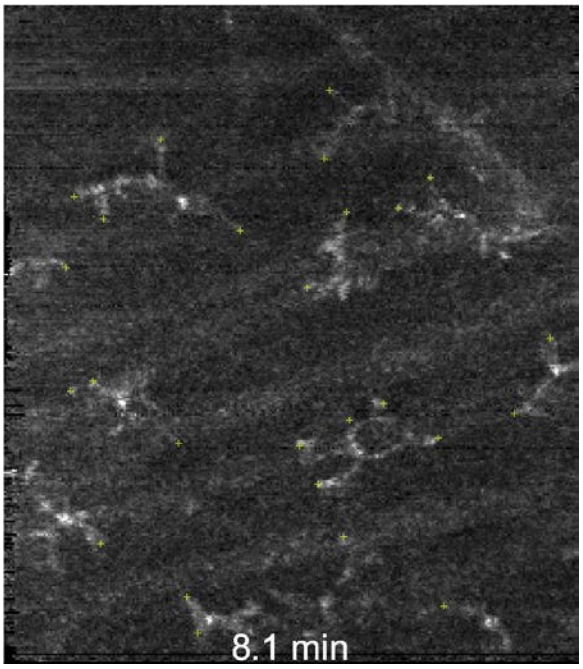

Movie S1. AO-OCT time-lapsed video over ~25 minutes of ILM macrophage cells with process endpoints marked (yellow crosses) from 33-year old control subject 8009. ILM macrophage dynamics are best visualized when movies are played in loop mode.

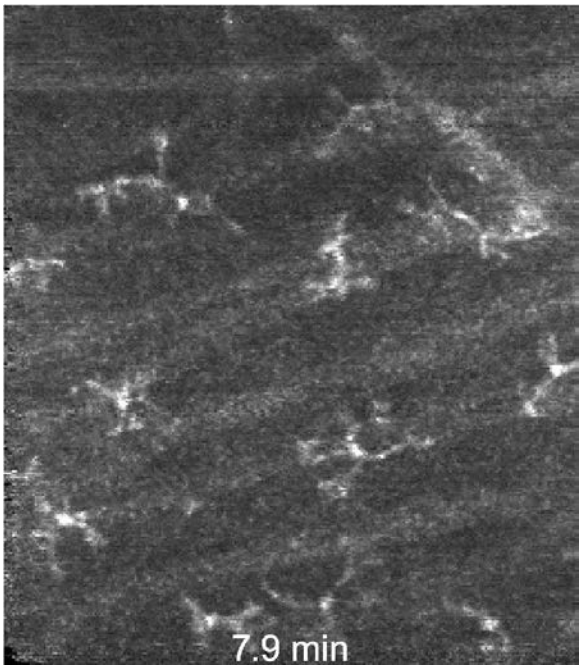

Movie S2. AO-OCT time-averaged video over ~25 minutes of ILM macrophage cells from control subject 8009.

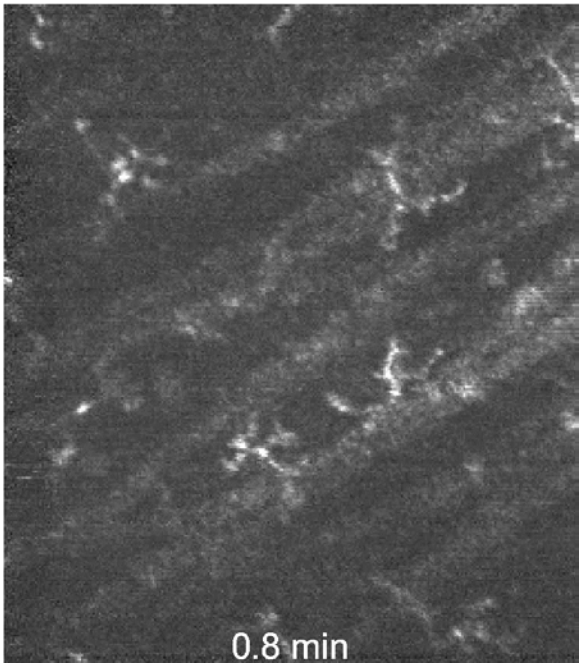

Movie S3. AO-OCT time-averaged video over ~20 minutes of ILM macrophage cells from 35-year old control subject 6581.

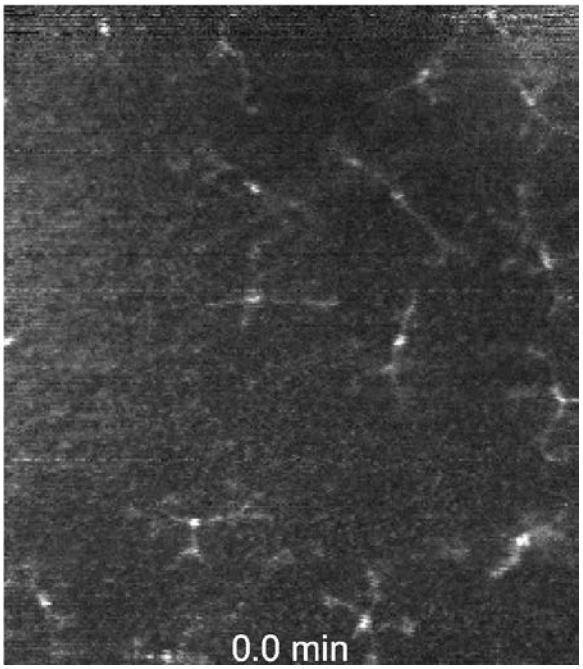

Movie S4. AO-OCT time-averaged video over ~25 minutes of ILM macrophage cells from 24-year old control subject 8851.

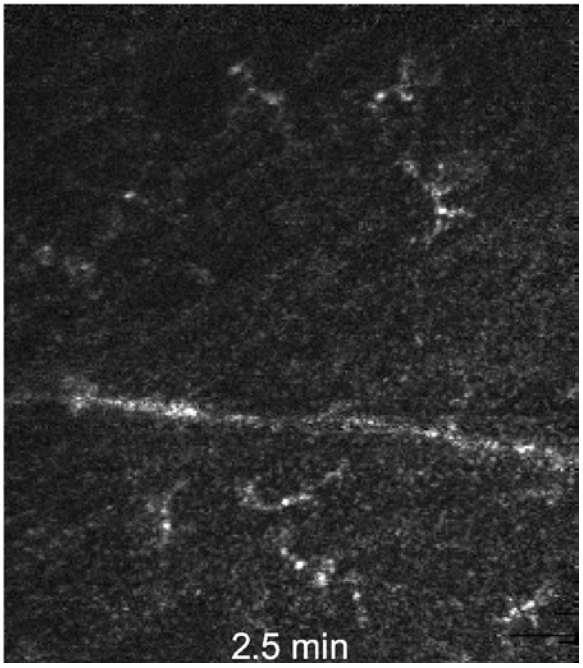

Movie S5. AO-OCT time-lapsed video over ~5 minutes of ILM macrophage cells from 52-year old glaucoma subject 1733.